DROUGHT

Large contribution from anthropogenic warming to an emerging North American megadrought

A. Park Williams[1]*, Edward R. Cook[1], Jason E. Smerdon[1], Benjamin I. Cook[1,2], John T. Abatzoglou[3,4], Kasey Bolles[1], Seung H. Baek[1,5], Andrew M. Badger[6,7,8], Ben Livneh[6,9]

Severe and persistent 21st-century drought in southwestern North America (SWNA) motivates comparisons to medieval megadroughts and questions about the role of anthropogenic climate change. We use hydrological modeling and new 1200-year tree-ring reconstructions of summer soil moisture to demonstrate that the 2000–2018 SWNA drought was the second driest 19-year period since 800 CE, exceeded only by a late-1500s megadrought. The megadrought-like trajectory of 2000–2018 soil moisture was driven by natural variability superimposed on drying due to anthropogenic warming. Anthropogenic trends in temperature, relative humidity, and precipitation estimated from 31 climate models account for 46% (model interquartiles of 34 to 103%) of the 2000–2018 drought severity, pushing an otherwise moderate drought onto a trajectory comparable to the worst SWNA megadroughts since 800 CE.

S outhwestern North America (SWNA; western United States and northern Mexico: 30°N to 45°N, 105°W to 125°W) has been anomalously dry and warm in the 21st century relative to the 20th century (1–3). The 21st-century drought severity has been reflected in reduced snowpack (4), reduced river flow and lake levels (5), declines in groundwater availability (6, 7), shifts in agricultural activities (8), forest drought stress (9), increased wildfire activity (10), and reduced vegetation carbon uptake (11).

Paleoclimatic proxies indicate that SWNA experienced many severe swings in hydroclimate before the observed period. In particular, tree-ring records reveal several megadrought events during the Medieval era and subsequent centuries (~850–1600 CE) that dwarfed all droughts in the following 400 years in intensity and duration (12). These megadroughts were likely associated with cool eastern tropical Pacific sea surface temperatures, which promote an atmospheric wave train that blocks Pacific storms from reaching SWNA (13–15). Any attribution of recent drought to anthropogenic climate change must consider this region's capacity for large internal hydroclimatic variability (16, 17). Although 21st-century drought conditions have been clearly promoted by natural Pacific Ocean variability (18–20), certain elements are also consistent with projected drying due to anthropogenic radiative forcing (21–23). Cold-season precipitation deficits across the southwestern United States and northern Mexico are consistent with modeled poleward expansion of the subtropics, albeit with large uncertainties in models and observations (24, 25). Observed warming since the early 1900s is more uniformly consistent with model simulations of anthropogenic trends, decreasing SWNA runoff and warm-season soil moisture by reducing snowpack and increasing evaporative demand (26–28). Models project that 21st-century SWNA summer droughts will intensify owing to declining spring precipitation in the southern portion of the region and continued warming-induced reductions of summer runoff and soil moisture (22–24, 29).

Here, we use 1521 tree-ring chronologies to reconstruct 0- to 200-cm summer (June to August) soil moisture and snow water equivalent (hereinafter termed "soil moisture" collectively) anomalies on a 0.5° latitude-longitude grid back to 800 CE across western North America [(30); Fig. 1]. Soil-moisture anomalies are standardized relative to the entire 800–2018 CE period, and the magnitude of negative anomalies indicates drought severity. The soil-moisture record targeted in the reconstruction covers 1901–2018 and is referred to as Noah-calibrated soil moisture (31). Because true observations of soil moisture do not exist, this soil-moisture record is modeled based on observed climate. Monthly precipitation, temperature, humidity, wind speed, and radiation data are used to force a bucket-type water-balance model with intermonth persistence tuned to emulate the Community Noah land-surface model (32) (fig. S1). The reconstruction method is the same method that has been used to develop previous continental drought atlases (16). Reconstruction skill is evaluated as the squared Pearson's correlation (R^2) between observations during the 1901–1983 calibration period and out-of-sample reconstruction values that were calculated by using leave-10-out cross-validation (30). Reconstruction skill is highly significant ($P < 0.01$) across much of SWNA (Fig. 1A). The cross-validated R^2 for the SWNA regionally averaged reconstruction is 0.86 back to 1700 CE (Fig. 1B). Skill reduces back in time owing to loss of tree-ring chronologies but remains above 0.73, even when using the subset of tree-ring chronologies extending back to 800 CE (Fig. 1B).

We evaluated 19-year running means of reconstructed and observed soil-moisture anomalies for explicit contextualization of the dry 2000–2018 period. Running-mean values are assigned to the final year in each 19-year window. During 800–2018 CE, there were 35 prolonged drought events with more than one negative SWNA 19-year running-mean soil-moisture anomaly. We rank the severity of each prolonged drought event based on the event's most negative 19-year soil-moisture anomaly. Definitions of megadrought vary, but in North America, they generally refer to multidecade drought events that contained periods of very high severity and were longer lasting than any event observed in the 19th or 20th centuries (12). Here we identify the strongest SWNA megadroughts in the reconstruction as the prolonged drought events that contained at least one 19-year anomaly that was 0.25 standard deviations (σ) more negative than any observed in the 20th century. The regionally averaged SWNA reconstruction (Fig. 1C) reveals four megadroughts that satisfy this criterion in the late 800s, mid-1100s, late 1200s, and late 1500s.

The 21st-century prolonged drought event (still ongoing as of 2020 given our definition) registered its first negative SWNA 19-year anomaly in 1996–2014, and its most negative anomaly (2000–2018) was −0.76 σ; the late-1500s megadrought was the only reconstructed event with a more negative 19-year soil-moisture anomaly than that in 2000–2018 (Fig. 1C). The most severe SWNA 19-year soil moisture anomaly during the late-1500s megadrought was −0.82 σ in 1575–1593. The 2000–2018 drought severity was nevertheless within the uncertainty ranges of several other 19-year drought severities, and the late-1500s event contained six 19-year anomalies more negative than that in 2000–2018. Within SWNA, local drought rankings during the 21st-century event were generally not as high as the ranking of the regionally averaged drought (Fig. 1D). Only 38.5% of SWNA experienced a local 19-year drought severity that ranked among the top five since 800 CE, a smaller aerial extent of high-ranking drought than occurred

[1]Lamont-Doherty Earth Observatory of Columbia University, Palisades, NY 10964, USA. [2]NASA Goddard Institute for Space Studies, New York, NY 10025, USA. [3]Department of Geography, University of Idaho, Moscow, ID 83844, USA. [4]Management of Complex Systems Department, UC Merced, Merced, CA 95343, USA. [5]Department of Earth and Environmental Sciences, Columbia University, New York, NY 10027, USA. [6]Cooperative Institute for Research in Environmental Sciences, University of Colorado Boulder, Boulder, CO 80302, USA. [7]Universities Space Research Association, Columbia, MD 21046, USA. [8]NASA Goddard Space Flight Center, Greenbelt, MD, USA 20771, USA. [9]Civil, Environmental, and Architectural Engineering, University of Colorado Boulder, Boulder, CO 80309, USA.
*Corresponding author. Email: williams@ldeo.columbia.edu

during the megadroughts of the mid-1100s, late 1200s, or late 1500s (Fig. 1D). Notably, the four megadroughts in Fig. 1 were longer than the 21st-century drought thus far, giving grid cells more chances to register high-ranking 19-year drought severities. Conversely, the 21st-century drought is the only event in which all SWNA grid cells registered at least one below-average 19-year soil-moisture anomaly.

The above results are consistent across alternate reconstructions with longer calibration periods that extend beyond 1983 (using fewer tree-ring records), with 2000–2018 always ranking second driest (fig. S2A). The above results are also consistent with alternate reconstructions of the self-calibrated Palmer Drought Severity Index [scPDSI; (33)] and soil-moisture simulated by the Variable Infiltration Capacity hydrological model [VIC; (34)], but the reconstruction targeting VIC soil moisture has considerably less skill than the reconstructions targeting Noah-calibrated soil moisture or scPDSI [(30); fig. S2, B and C]. The alternate reconstructions of scPDSI and VIC soil moisture agree with our primary reconstruction in placing 2000–2018 within the two most severe

prolonged SWNA droughts in at least 1200 years (fig. S2, B and C).

To address the contribution of anthropogenic climate change, we evaluated 1901–2018 trends in precipitation, temperature, and relative humidity simulated with 31 climate models in the fifth phase of the Coupled Model Intercomparison Project (CMIP5). During 2000–2018, the multimodel mean anthropogenic warming in SWNA was 1.2°C [model interquartiles (IQs): 1.0° to 1.5°C], with all models simulating warming (Fig. 2A). Anthropogenic warming increased the annual mean atmospheric vapor-pressure deficit by 9.6% (IQs: 8.4 to 11.3%), which increased the mean annual total evaporative demand (as estimated by the Penman-Monteith reference evapotranspiration) by 59 mm, or 4.5% (IQs: 53 to 73 mm, 4.1 to 5.5%) (Fig. 2, B and C). Models disagree on anthropogenic precipitation trends, with a slight multimodel mean increase in the SWNA annual total (6 mm, 1.2%; IQs: –6 to 12 mm, –2.5 to 2.2%) (Fig. 2D).

In Fig. 2, E to H, we estimate the effect of these anthropogenic climate trends on soil moisture as the difference between observed

soil-moisture anomalies and those recalculated after removing model-estimated anthropogenic trends from the observed climate records [e.g., (3, 10)]. The positive effect of the slight multimodel mean precipitation increase in northern SWNA (Fig. 2E) is overwhelmed by the spatially ubiquitous drying effect of increasing vapor-pressure deficit simulated by all models (Fig. 2F). Notably, the high intermodel spread in anthropogenic precipitation trends causes high spread among estimated soil-moisture trends (Fig. 2, D and E), and the true uncertainty may be even larger than suggested here owing to systematic model biases (25, 35). Combined, the multimodel mean estimates of anthropogenic trends in precipitation, temperature, and humidity force a 2000–2018 SWNA regionally averaged summer soil-moisture anomaly of –0.35 σ (IQs: –0.26 to –0.78 σ) (Fig. 2G). This accounts for 46% (IQs: 34 to 103%) of the observed anomaly (Fig. 2H). Of the 31 CMIP5 models considered, 28 (90%) simulated climate trends that promoted SWNA drought during 2000–2018 based on our water-balance estimates. Twenty-five models (81%) indicated that this altered baseline in mean climate

Fig. 1. Summer soil-moisture reconstruction for SWNA. (**A**) Cross-validated reconstruction skill (R^2) using tree-ring records that extend to 800 and 1700 CE (green contour: $R^2 \geq 0.5$; gray: reconstruction does not extend to 800 CE; yellow box: SWNA). (**B**) Time-resolved cross-validated R^2 of the SWNA regional reconstruction. The inset shows observations versus cross-validated reconstructions during the 1901–1983 calibration interval using tree-ring records extending back to 800 and 1700 CE. (**C**) Time series of reconstructed (red) and observed (blue) 19-year running-mean standardized SWNA soil moisture (gray: 95% reconstruction confidence interval; blue horizontal line: 2000–2018 mean; pink and green shading: the five drought and pluvial periods with the most-negative and most-positive 19-year soil-moisture anomalies, respectively).

(**D**) Maps of the local rank of the most negative 19-year anomaly to occur during each of the five drought events highlighted in (C). In the maps, the aqua color indicates no negative 19-year anomaly, and numbers in the top left corners indicate the rank of the most negative regionally averaged 19-year anomaly during each drought event.
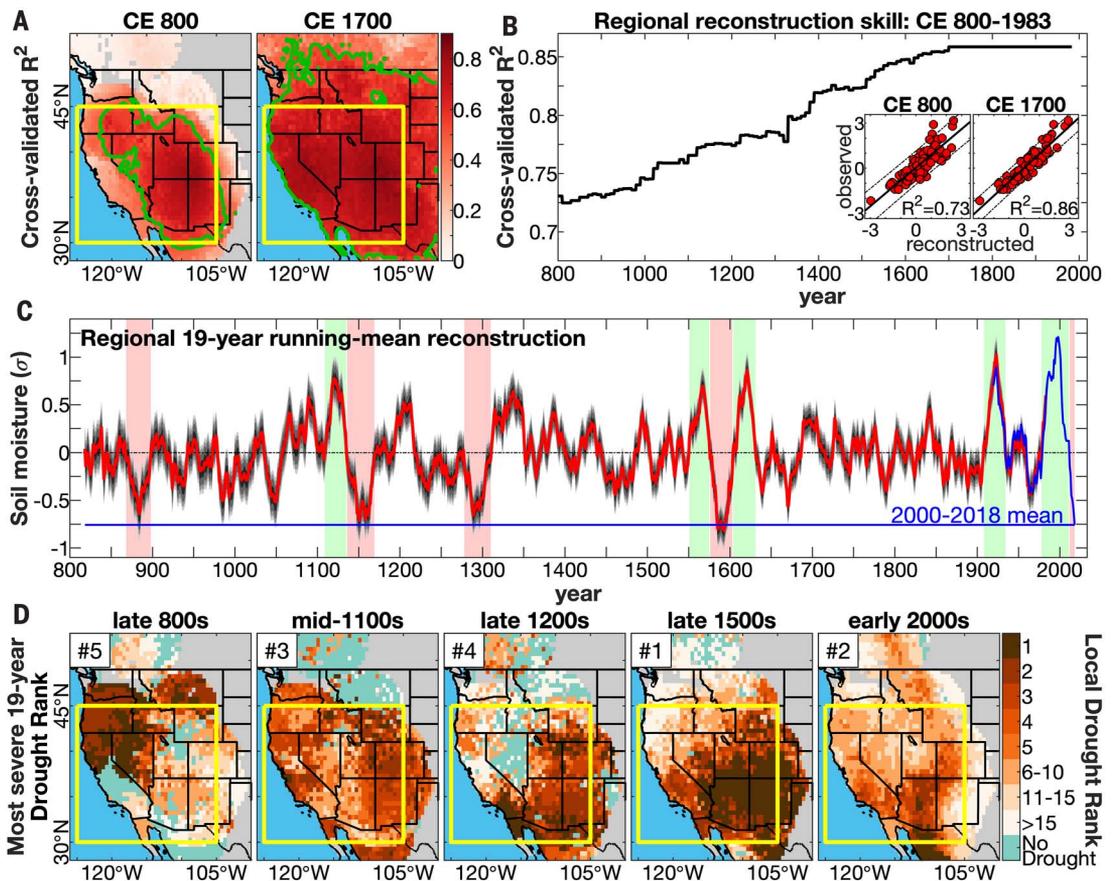
Fig. 2. Effects of anthropogenic climate trends.
(**A** to **G**) Time series plots showing the 19-year running-mean observed anomalies (black lines) in SWNA (yellow box in maps) for mean annual temperature (T) (A), mean annual vapor pressure deficit (VPD) (B), annual reference evapotranspiration (ETo) (C), annual precipitation (P) (D), and soil moisture [(E) to (G)]. Solid and dotted colored lines represent 19-year running-mean CMIP5 multimodel mean and IQ trends, respectively (gray lines: trends from 31 models). CMIP5 trends are evaluated for P, T, and relative humidity (RH). In (E) to (G), CMIP5 trends show contributions to observed soil-moisture anomalies since 1901. The maps show CMIP5 multi-model mean contributions to 2000–2018 anomalies (dots: >75% model agreement on sign; gray: masked out because reconstruction does not extend to 800 CE).
(**H**) Percent contribution of CMIP5 (bars) multimodel mean climate trends to the 2000–2018 SWNA soil-moisture anomaly (whiskers: model IQs). Anomalies are relative to 1921–2000 in (A) to (D) and 800–2018 CE in (E) to (G).
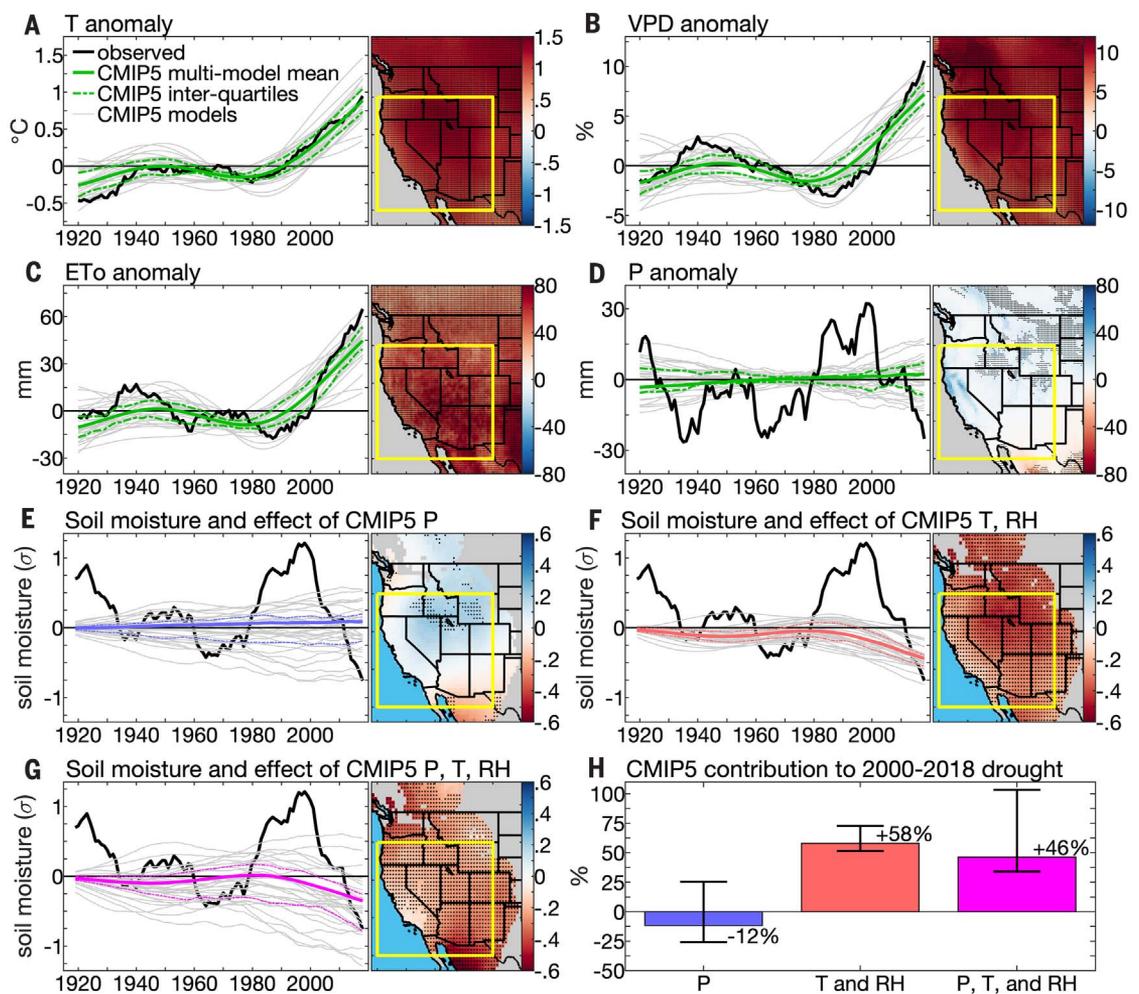
Fig. 3. Development of the most severe 19-year droughts since 800 CE. Time series of cumulative SWNA summer soil-moisture anomalies for the 20 prolonged droughts with the most-negative 19-year soil-moisture anomalies. The drought periods analyzed here begin 18 years before the most-negative 19-year anomaly. The dark blue line shows 2000–2018 cumulative anomalies after removing CMIP5 multimodel mean climate trends. The shaded regions represent 95% confidence intervals for the four reconstructed megadroughts shown with the light colored lines.
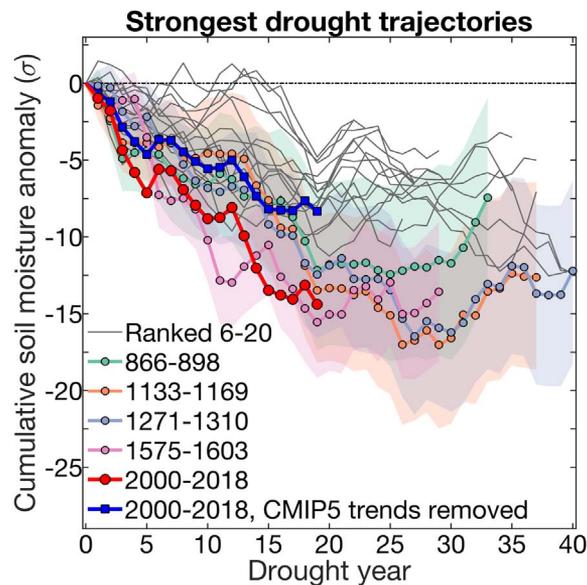
accounted for >25% of the observed 2000–2018 SWNA soil-moisture anomaly. This net anthropogenic drying effect is corroborated by the tree-ring records themselves. Reconstruction of an alternate summer soil-moisture record recalculated after removal of CMIP5 ensemble mean temperature and relative humidity trends reduces validation skill because the recalculated soil moisture is too wet relative to the reconstruction in recent decades (fig. S3).

When repeated for scPDSI and VIC soil moisture, the CMIP5 multimodel mean contribution to SWNA 2000–2018 drought severity was 46 and 30%, respectively (fig. S4). The weaker anthropogenic drying effect in the VIC simulation was primarily due to desert areas: (i) In high desert, warming reduces winter snow sublimation and increases infiltration; (ii) where vegetation is sparse, increased winter precipitation and minimal transpiration enhance deep moisture storage; and (iii) in more vegetated desert areas, soils dry to the

Fig. 4. Trends in summer soil moisture simulated directly from coupled models. (**Left**) CMIP5 19-year running-mean 0- to 200-cm summer soil-moisture anomalies for historical (1850–2005) and 21st-century (2006–2018) scenarios (standardization relative to 1850–2018; gray represents 26 models; brown represents multi-model mean, IQs). (**Right**) Multimodel mean anomalies in 2000–2018 (dots represent >75% model agreement on sign; yellow box indicates SWNA).

CMIP5 0-200 cm summer soil moisture
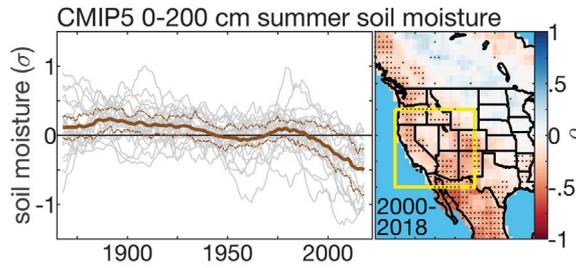
wilting point in summer regardless of anthropogenic climate trends, erasing all soil-moisture memory of warming-induced drying in spring (supplementary text S1 and figs. S5 to S10). Outside of deserts, and particularly in forested areas, the VIC model simulates summer soil drying driven by anthropogenic warming through enhanced evapotranspiration and early loss of snowpack (fig. S11).

Given known disagreement among land-surface models in deserts where small anomalies are substantial relative to dry climatologies (36) and the inherently better representation of forested areas by the tree-ring network, we repeated our reconstructions to target forested areas only. All forest-only reconstructions still estimate 2000–2018 to be among the two driest 19-year drought periods since 800 CE for SWNA (fig. S12, A to C). Considering SWNA forested areas only, the contribution of anthropogenic climate trends to 2000–2018 drought severity increased slightly for Noah-calibrated soil moisture and scPDSI (to 57 and 51%, respectively) and dramatically (to 83%) for VIC soil moisture (fig. S12, D to F). This stronger anthropogenic effect in the VIC simulation is likely due to the additional effect of warming-driven snowpack loss, which is not accounted for directly in the Noah-calibrated soil moisture or scPDSI. The VIC simulations indicate a steady warming-driven reduction to SWNA spring snowpack over the past century that accounts for the majority of the simulated spring snowpack anomaly in 2000–2018 (fig. S13).

The 2000–2018 drought was preceded by the wettest 19-year period (1980–1998) in at least 1200 years (Fig. 1C). Climate models project enhanced precipitation variability across much of the globe as a result of anthropogenic climate change, and this includes a slight 21st-century trend toward greater decadal precipitation swings in SWNA (37). This tendency is also apparent in model simulations of summer 0- to 200-cm soil moisture, but this simulated effect does not emerge until the second half of the 21st century (fig. S14). Regardless of the anthropogenic impact on multidecadal variability, the 1980–2018 wet-to-dry transition was hastened by the background drying forced from anthropogenic warming.

Figure 3 shows that the 2000–2018 drought was on a megadrought-like trajectory throughout its development. In the absence of anthropogenic climate trends, 2000–2018 would still rank among the 11 most severe prolonged droughts in the reconstruction (dark blue line in Fig. 3), but anthropogenic warming was critical for placing 2000–2018 on a trajectory consistent with the most severe past megadroughts. These results are robust regardless of the drought metric used or whether only forested areas are considered (fig. S15).

The results above do not account for the possibility that increased atmospheric carbon dioxide concentration ($[CO_2]$) has ameliorated soil-water loss by allowing plants to reduce stomatal conductance and use water more efficiently through increased surface resistance (r_s) to transpiration (38). Although the effects of enhanced $[CO_2]$ on vegetation and surface water fluxes are highly uncertain (39), we explore how our results would be affected by a r_s response to $[CO_2]$ as simulated by current Earth system models. Repeating our study with an adjusted calculation of reference evapotranspiration that assumes the CMIP5 multimodel mean r_s response to $[CO_2]$ (40) reduces 2000–2018 drought severity by about 18% (to −0.62 σ). This prolonged drought ranks fifth in the revised reconstruction, still in line with the megadroughts (fig. S16). Even with the assumed increase in r_s, 30% of the 2000–2018 drought's severity is attributed to anthropogenic climate trends, with 81% of models simulating some degree of anthropogenic drying. Importantly, the potency of the $[CO_2]$ effect on r_s varies by a factor of three among CMIP5 models (40), highlighting considerable uncertainty in this effect.

Our relatively simple hydrological modeling approach also does not account for coupled land-atmosphere interactions or dynamic vegetation responses to climate. It has been argued that hydrological effects of anthropogenic climate change are better addressed with coupled Earth system models that directly simulate land-atmosphere coupling and vegetation responses to changes in climate and $[CO_2]$ (38, 41). Figure 4 shows that, of the 26 CMIP5 models with soil-moisture data available for historical and 21st-century climate scenarios, 23 (88%) simulate negative soil-moisture

anomalies in SWNA during 2000–2018, with a multimodel mean of −0.50 σ (IQs: −1.38 to −0.17 σ) relative to a 1850–2018 CE baseline. Because each model simulation has its own internal climate variability, intermodel agreement on dry soil during 2000–2018 arises from the common anthropogenic forcing. The multimodel mean 2000–2018 anomaly derived directly from CMIP5 soil-moisture simulations is somewhat larger than the anthropogenic effect of −0.40 σ found when the previously calculated anthropogenic effect shown in Fig. 2G is rescaled relative to 1850–2018 CE. The stronger anthropogenic soil drying simulated by the CMIP5 models is likely due to reduced spring-summer mountain snowpack and enhanced vegetation water use caused by lengthened growing seasons and increased leaf area due to CO_2 fertilization (39). Notably, the simulated ability for vegetation to survive and perpetuate these modeled soil-moisture declines may be unrealistic because current Earth system models inadequately represent nutrient and moisture limitations on vegetation activity (42–44).

The tree-ring record serves as an ominous reminder that natural climate variability can drive SWNA megadroughts that are as severe and longer than the 21st-century drought thus far. The atmosphere and ocean anomalies that drove past megadroughts very likely dwarfed those that occurred during 2000–2018, but superposition of the 2000–2018 climate dynamics on background anthropogenic soil drying put an otherwise moderately severe soil-moisture drought onto a trajectory characteristic of the megadroughts of 800–1600 CE. Critical to the megadrought-like trajectory of the 21st-century event were enhanced evaporative demand, early snowpack loss, and a broad spatial extent, all promoted by anthropogenic warming. Natural variability may very well end the early 21st-century drought in the coming years, and this transition may be under way after a wet 2019. However, our work demonstrates that the magnitude of background anthropogenic soil drying is already substantial relative to the range of natural multidecadal variability. Furthermore, anthropogenic global warming and its drying influence in SWNA are likely still in their infancy. The magnitude of future droughts in North America and elsewhere will depend greatly on future rates of anthropogenic greenhouse gas emissions globally. The effects of future droughts on humans will be further dependent on sustainable resource use because buffering mechanisms such as ground water and reservoir storage are at risk of being depleted during dry times.

REFERENCES AND NOTES

1. K. M. Andreadis, E. A. Clark, A. W. Wood, A. F. Hamlet, D. P. Lettenmaier, *J. Hydrometeorol.* **6**, 985–1001 (2005).
2. M. Hoerling *et al.*, *Bull. Am. Meteorol. Soc.* **95**, 269–282 (2014).

3. A. P. Williams *et al.*, . *Geophys. Res. Lett.* **42**, 6819–6828 (2015).
4. P. W. Mote, S. Li, D. P. Lettenmaier, M. Xiao, R. Engel, *NPJ Clim. Atmos. Sci.* **1**, 2 (2018).
5. M. Xiao, B. Udall, D. P. Lettenmaier, *Water Resour. Res.* **54**, 6739–6756 (2018).
6. M. Rodell *et al.*, *Nature* **557**, 651–659 (2018).
7. C. C. Faunt, M. Sneed, J. Traum, J. T. Brandt, *Hydrogeol. J.* **24**, 675–684 (2016).
8. R. Howitt, J. Medellin-Azuara, D. MacEwan, J. Lund, D. A. Sumner, "Economic analysis of the 2014 drought for California agriculture" (UC Davis Center for Watershed Sciences, Davis, CA, 2014).
9. A. P. Williams *et al.*, *Nat. Clim. Chang.* **3**, 292–297 (2013).
10. J. T. Abatzoglou, A. P. Williams, *Proc. Natl. Acad. Sci. U.S.A.* **113**, 11770–11775 (2016).
11. C. R. Schwalm *et al.*, *Nat. Geosci.* **5**, 551–556 (2012).
12. B. I. Cook *et al.*, *Wiley Interdiscip. Rev. Clim. Change* **7**, 411–432 (2016).
13. R. Seager *et al.*, *Quat. Sci. Rev.* **26**, 2322–2336 (2007).
14. B. I. Cook *et al.*, *J. Geophys. Res. Atmos.* **123**, 11307–11320 (2019).
15. N. J. Steiger *et al.*, *Sci. Adv.* **5**, eaax0087 (2019).
16. E. R. Cook *et al.*, *J. Quaternary Sci.* **25**, 48–61 (2010).
17. C. A. Woodhouse, D. M. Meko, G. M. MacDonald, D. W. Stahle, E. R. Cook, *Proc. Natl. Acad. Sci. U.S.A.* **107**, 21283–21288 (2010).
18. T. L. Delworth, F. Zeng, A. Rosati, G. A. Vecchi, A. T. Wittenberg, *J. Clim.* **28**, 3834–3845 (2015).
19. R. Seager, M. Ting, *Curr. Clim. Change Rep.* **3**, 141–149 (2017).
20. F. Lehner, C. Deser, I. R. Simpson, L. Terray, *Geophys. Res. Lett.* **45**, 6251–6261 (2018).
21. R. Seager *et al.*, *Science* **316**, 1181–1184 (2007).
22. B. I. Cook, T. R. Ault, J. E. Smerdon, *Sci. Adv.* **1**, e1400082 (2015).
23. T. R. Ault, J. S. Mankin, B. I. Cook, J. E. Smerdon, *Sci. Adv.* **2**, e1600873 (2016).
24. M. Ting, R. Seager, C. Li, H. Liu, N. Henderson, *J. Clim.* **31**, 4265–4279 (2018).
25. R. Seager *et al.*, *Nat. Clim. Chang.* **9**, 517–522 (2019).
26. T. P. Barnett *et al.*, *Science* **319**, 1080–1083 (2008).
27. G. J. McCabe, D. M. Wolock, G. T. Pederson, C. A. Woodhouse, S. McAfee, *Earth Interact.* **21**, 1–14 (2017).
28. P. C. D. Milly, K. A. Dunne, *Science* **367**, 1252–1255 (2020).
29. D. R. Cayan *et al.*, *Proc. Natl. Acad. Sci. U.S.A.* **107**, 21271–21276 (2010).
30. Materials and methods are available as supplementary materials.
31. A. P. Williams *et al.*, *J. Geophys. Res. Atmos.* **122**, 10888–10905 (2017).
32. M. B. Ek *et al.*, *J. Geophys. Res. Atmos.* **108**, 8851 (2003).
33. N. Wells, S. Goddard, M. J. Hayes, *J. Clim.* **17**, 2335–2351 (2004).
34. X. Liang, D. P. Lettenmaier, E. F. Wood, S. J. Burges, *J. Geophys. Res. Atmos.* **99**, 14415–14428 (1994).
35. I. R. Simpson, R. Seager, M. Ting, T. A. Shaw, *Nat. Clim. Chang.* **6**, 65–70 (2016).
36. R. D. Koster *et al.*, *J. Clim.* **22**, 4322–4335 (2009).
37. A. G. Pendergrass, R. Knutti, F. Lehner, C. Deser, B. M. Sanderson, *Sci. Rep.* **7**, 17966 (2017).
38. A. L. S. Swann, F. M. Hoffman, C. D. Koven, J. T. Randerson, *Proc. Natl. Acad. Sci. U.S.A.* **113**, 10019–10024 (2016).
39. J. S. Mankin, R. Seager, J. E. Smerdon, B. I. Cook, A. P. Williams, *Nat. Geosci.* **12**, 983–988 (2019).
40. Y. Yang, M. L. Roderick, S. Zhang, T. R. McVicar, R. J. Donohue, *Nat. Clim. Chang.* **9**, 44–48 (2019).
41. A. Berg, J. Sheffield, *Curr. Clim. Change Rep.* **4**, 180–191 (2018).
42. W. K. Smith *et al.*, *Nat. Clim. Chang.* **6**, 306–310 (2015).
43. W. R. Wieder, C. C. Cleveland, W. K. Smith, K. Todd-Brown, *Nat. Geosci.* **8**, 441–444 (2015).
44. W. Yuan *et al.*, *Sci. Adv.* **5**, eaax1396 (2019).
45. P. Williams, Large contribution from anthropogenic warming to an emerging North American megadrought (NCEI Accession 0209529). NOAA National Centers for Environmental Information (2020); doi:10.25921/2vbe-8092.

Science

Large contribution from anthropogenic warming to an emerging North American megadrought

A. Park Williams, Edward R. Cook, Jason E. Smerdon, Benjamin I. Cook, John T. Abatzoglou, Kasey Bolles, Seung H. Baek, Andrew M. Badger and Ben Livneh

A trend of warming and drying

Global warming has pushed what would have been a moderate drought in southwestern North America into megadrought territory. Williams *et al.* used a combination of hydrological modeling and tree-ring reconstructions of summer soil moisture to show that the period from 2000 to 2018 was the driest 19-year span since the late 1500s and the second driest since 800 CE (see the Perspective by Stahle). This appears to be just the beginning of a more extreme trend toward megadrought as global warming continues.

Science, this issue p. 314; see also p. 238

ARTICLE TOOLS	http://science.sciencemag.org/content/368/6488/314
SUPPLEMENTARY MATERIALS	http://science.sciencemag.org/content/suppl/2020/04/15/368.6488.314.DC1
RELATED CONTENT	http://science.sciencemag.org/content/sci/368/6488/254.full http://science.sciencemag.org/content/sci/368/6488/226.full http://science.sciencemag.org/content/sci/368/6488/234.full http://science.sciencemag.org/content/sci/368/6488/256.full http://science.sciencemag.org/content/sci/368/6488/261.full http://science.sciencemag.org/content/sci/368/6488/266.full http://science.sciencemag.org/content/sci/368/6488/270.full http://science.sciencemag.org/content/sci/368/6488/274.full http://science.sciencemag.org/content/sci/368/6488/238.full http://science.sciencemag.org/content/sci/368/6488/250.full http://science.sciencemag.org/content/sci/368/6488/251.1.full http://science.sciencemag.org/content/sci/368/6488/251.2.full http://science.sciencemag.org/content/sci/368/6488/252.full http://science.sciencemag.org/content/sci/370/6516/eabf3676.full
REFERENCES	This article cites 89 articles, 17 of which you can access for free http://science.sciencemag.org/content/368/6488/314#BIBL

Use of this article is subject to the Terms of Service